

Accepted Manuscript

Mechanical properties of an Al-Zn-Mg alloy processed by ECAP and heat treatments

Mohamed A. Afifi, Ying Chun Wang, Pedro Henrique R. Pereira, Yi Huang, Yangwei Wang, Xingwang Cheng, Shukui Li, Terence G. Langdon



PII: S0925-8388(18)32842-1

DOI: [10.1016/j.jallcom.2018.07.343](https://doi.org/10.1016/j.jallcom.2018.07.343)

Reference: JALCOM 47059

To appear in: *Journal of Alloys and Compounds*

Received Date: 12 June 2018

Revised Date: 27 July 2018

Accepted Date: 30 July 2018

Please cite this article as: M.A. Afifi, Y.C. Wang, P.H.R. Pereira, Y. Huang, Y. Wang, X. Cheng, S. Li, T.G. Langdon, Mechanical properties of an Al-Zn-Mg alloy processed by ECAP and heat treatments, *Journal of Alloys and Compounds* (2018), doi: 10.1016/j.jallcom.2018.07.343.

This is a PDF file of an unedited manuscript that has been accepted for publication. As a service to our customers we are providing this early version of the manuscript. The manuscript will undergo copyediting, typesetting, and review of the resulting proof before it is published in its final form. Please note that during the production process errors may be discovered which could affect the content, and all legal disclaimers that apply to the journal pertain.

Mechanical properties of an Al-Zn-Mg alloy processed by ECAP and heat treatments

Mohamed A. Afifi^a, Ying Chun Wang^{a,b *}, Pedro Henrique R. Pereira^{c,d}, Yi Huang^c, Yangwei Wang^{a,b}, Xingwang Cheng^{a,b}, Shukui Li^{a,b}, Terence G. Langdon^c

^aSchool of Materials Science and Engineering, Beijing Institute of Technology, Beijing 100081, China

^bNational Key Laboratory of Science and Technology on Materials under Shock and Impact, Beijing 100081, China

^cMaterials Research Group, Faculty of Engineering and the Environment, University of Southampton,
Southampton SO17 1BJ, UK

^d Department of Metallurgical and Materials Engineering, Universidade Federal de Minas Gerais,
Belo Horizonte, MG 31270-901, Brazil

*Corresponding author: Ying Chun Wang, e-mail: wangyc@bit.edu.cn; Tel: +861068913937 ext.801

Abstract

An investigation was conducted to study the influence of equal-channel angular pressing (ECAP) and post-ECAP aging at 393 K for 20 h on the microstructures and tensile properties of a supersaturated Al-Zn-Mg alloy together with the effect of pre-ECAP heat treatments on the mechanical properties of the alloy after ECAP and after post-ECAP heat treatments. The results show that during ECAP processing for up to 4 passes for the supersaturated Al alloy there is a simultaneous occurrence of grain refinement, increases in the dislocation density and dynamic aging precipitation forming large numbers of fine spherical well-distributed precipitates which enhance the yield strength but decrease the ductility. During post-ECAP aging, there is a limited dislocation recovery with slight grain growth and the precipitate sizes increase together with the formation of a few larger platelet precipitates and the transformation of G.P. zones to η' and η' to η leading to a strength reduction after 4 passes of ECAP. The precipitates in the ECAP-processed alloy with pre-ECAP in the supersaturated state formed through dynamic aging precipitation are higher in their volume fraction, smaller in their size and more homogeneously distributed in the Al matrix than those in the alloy with pre-ECAP in the peak aging state which mainly come from the fragmented η' existing in the matrix before ECAP. The strengths of the alloy both after ECAP processing and after post-ECAP heat treatments with pre-ECAP in the supersaturation state are higher than with pre-ECAP in the peak aging state.

Keywords: Al-Zn-Mg alloy; equal-channel angular pressing; post-ECAP aging; pre-ECAP heat treatments; tensile testing

1. Introduction

There are several different methods for strengthening metal alloys but introducing grain refinement to an ultrafine-grained (UFG) structure through processing through the application of severe plastic deformation (SPD) is one of the most successful techniques for improving the mechanical properties of polycrystalline alloys [1-6]. Although there are now a number of different SPD procedures, processing by equal-channel angular pressing (ECAP) is especially attractive because it uses reasonably large samples and it can be scaled-up relatively easily to produce bulk UFG materials that may be used for a range of structural applications [4,5]. Investigations of the ECAP processing of precipitation-hardened aluminum alloys, such as Al-Zn-Mg alloys, are of great importance because a combination of strain hardening and grain boundary strengthening, together with precipitation hardening during the ECAP processing, may further enhance their mechanical properties so that the alloys can be applied more extensively in a range of industrial applications [7-12].

Several reports are now available describing the evolution of the microstructures in Al-Zn-Mg-(Cu) alloys during ECAP processing and the influence of this evolution on the mechanical properties of the alloys [7, 11, 13-16]. For example, it was documented that processing by ECAP for 8 passes at 473 K promotes the precipitation of a fine spherical η phase in supersaturated Al-Zn-Mg alloys because the dislocations introduced by ECAP act as nucleation sites for precipitates [7]. The ECAP processing of an Al-Zn-Mg-Cu alloy in a solution heat-treated condition after 3 passes at 423 K showed an increase in hardness compared with ECAP processing after 1 pass due to the refined grains and the presence of spherical η' and η [11]. In another study, fine grains with an average size of ~150 nm were obtained in an Al-7075 alloy after 3 ECAP passes at 353 K or 8 passes at 403 K [13]. Furthermore, the tensile properties were improved under these ECAP processing conditions due to the significant grain refinement, the presence of fine second-phase particles and the high densities of dislocations [7, 13, 16].

It is now recognized that pre-ECAP and post-ECAP heat treatments also have significant influences on the microstructures and mechanical properties of Al-Zn-Mg-(Cu) alloys because, in addition to the ultrafine grains and the large numbers of dislocations produced by ECAP processing, the mechanical properties of these alloys are determined primarily by the precipitate characteristics, including their type, size, shape and distribution, which can be changed during appropriate heat treatments [9-10, 12, 17]. A study on an Al-Zn-Cu-Mg alloy subjected to different pre-ECAP heat treatments showed that the supersaturated Al alloy processed by ECAP for 3 passes followed by aging at 393 K for 16 h possessed higher tensile strengths and higher ductility compared to samples pre-ECAP annealed at 553 K for 5 h after ECAP processing with subsequent annealing at 743 K for 0.5 h and further aging at 393 K for 24 h [9]. The enhanced tensile properties were attributed to the equiaxed fine grains together with the high dislocation density and homogenous distribution of very fine precipitates with an average size of ~3.9 nm while the enhanced ductility was ascribed to the grain refinement [9].

In another study, an Al-Zn-Mg-Cu was subjected to four different heat treatments before or after ECAP processing [12]. It was found that a solid solution of the Al alloy annealed at 743 K for 1 h and then quenched in water followed by ECAP for 3-4 passes at 393 K gave the optimum mechanical properties due to the presence of fine G.P. zones and η' precipitates formed by dynamic aging with sizes in the range of 3-5 nm. An investigation of supersaturated Al-Zn-Mg-(Cu) alloys which were processed by ECAP for 1 pass at 428 K or 453 K followed by artificial aging at 373, 393 or 413 K with different aging times showed that the best strengthening was obtained after post-ECAP aging at 373 K with an aging time of 20-30 h [17]. It was also reported that during ECAP processing the dislocation density increases and provides numerous sites for the heterogeneous nucleation of particles by dynamic aging precipitation and fast paths for diffusion and particle growth whereas after aging at 373 K for 30 h there is little change in the sub-grain structure and particle density but a slight increase in the average particle

size. These increases in both strength and ductility were also attributed to the sub-micrometer-sized grains, the high dislocation density and the finer and more homogenous precipitates [17].

A review of these data shows that pre- and post-ECAP heat treatments have significant influences on the mechanical properties of the Al-Zn-Mg-(Cu) alloys primarily because of the role of precipitation. However, to date there has been no comprehensive study systematically investigating either the relationship between microstructure and properties based on a control of the precipitation by pre- and post-ECAP heat treatments or the ECAP processing of an Al-Zn-Mg alloy which has Mn- and Cr-rich phase-forming elements. An earlier study examined the microstructure and tensile properties of an Al-Zn-Mg alloy with pre-ECAP in the peak aging state after ECAP processing and after post-ECAP heat treatments [18]. Nevertheless, the effect of ECAP processes and post-ECAP aging on the microstructure and mechanical properties of the Al-Zn-Mg alloy remains unclear with pre-ECAP in a supersaturation state. Consequently, the present investigation was initiated specifically to examine the influence of ECAP processing and post-ECAP aging on the supersaturated Al-Zn-Mg alloy and to fully elucidate the effects of pre-ECAP and post-ECAP heat treatments on the mechanical properties through microstructural analysis.

2. Experimental material and procedures

An Al-Zn-Mg alloy having a chemical composition (wt.%) of Al-4.53 Zn-2.52 Mg-0.35 Mn-0.2 Cr-0.11 Cu-0.1 Zr was received in a T6 state (solid solution treatment at 743 K for 1 h and peak aging at 393 K for 24 h) and it was cut into billets with diameters of 10 mm and lengths of 65 mm. Prior to ECAP, the billets were solid solution treated at 743 K for 1 h and then quenched in water. The ECAP was conducted for either 1 or 4 passes at a temperature of 423 K. Full details of the ECAP processing were given previously [18]. Following ECAP, samples were aged at 393 K for 20 h using a forced convection furnace and then cooled in air. The processing combining a solid solution heat treatment and

ECAP processing is hence forth designated SS-ECAP and the processing combining a solid solution heat treatment, ECAP processing and post-ECAP aging is designated SS-ECAP-HT. For convenience, the sample nomenclatures are summarized in Table 1 with the corresponding processing parameters.

Tensile testing was carried out at room temperature (RT, ~298 K) at an initial strain rate of $1.0 \times 10^{-3} \text{ s}^{-1}$ using a universal Instron 5966 testing machine. Planar dog-bone tensile samples were machined along the pressing direction with nominal gauge dimensions of $10 \times 2 \times 1.3 \text{ mm}^3$. At least two samples were tested for each condition to verify reproducibility. The microstructures were characterized by transmission electron microscopy (TEM) and high resolution transmission electron microscopy (HRTEM) using an F20 field emission microscope operating at 200 kV. The samples for TEM were prepared by mechanical grinding using grit papers with different particle sizes ranging from 1000 to 5000 mesh followed by thinning to electron transparency using a Gatan Dual Ion Milling System. The average particle sizes were measured by calculating the mean of ~500 particles in each condition. The average grain sizes of the samples were measured in TEM images by counting more than 150 intercepts using the circular intercept method following ASTM E112-12. In order to quantify the densities and volume fractions of precipitates, foil thickness measurements were performed using convergent beam electron diffraction (CBED) [19,20].

The dislocation densities were evaluated using the modified Williamson-Hall method with the aid of D8 Advanced Bruker X-ray diffraction (XRD) by calculating the crystallite size, d , and the microstrain, ε , of samples from the XRD peak broadening, B , using the equation [8,21]:

$$B \cos \theta_b = \frac{k\lambda}{d} + \varepsilon \sin \theta_b \quad (1)$$

where λ is the wavelength of the Cu K α radiation of 1.54 Å, k is a constant having a value of ~0.9 and θ_b is the Bragg angle [8]. Plotting $B \cos \theta_b$ against $\sin \theta_b$, the values of d and ε were obtained directly from

the slope and intercept of the fitted curve. The dislocation density was then evaluated from the relationship [22]:

$$\rho = \frac{2\sqrt{3}\varepsilon}{db} \quad (2)$$

where $b = 0.286$ nm is the magnitude of the Burgers vector for Al [23]. The crystallite size, d , and the microstrain, ε , were obtained from Eq. (1).

3. Experimental results

3.1 Tensile behavior

The tensile true stress-true strain curves of the as-received, the SS-ECAP processed and the SS-ECAP-HT treated Al-Zn-Mg alloy are shown in Fig. 1. It is apparent that the as-received material which is in the T6 state has the highest work hardening capability and the best ductility. After SS-ECAP processing for 1 pass, the alloy maintains the work hardening until fracture at a true strain of ~0.12. However, for the sample after SS-ECAP for 4 passes, close inspection of Fig. 1 shows there is work hardening up to a true strain of ~0.05 and then work softening until fracture. In addition, the SS-ECAP processing enhances the yield strength by comparison with the as-received sample and when the number of ECAP passes increases from 1 to 4 the yield strength also increases significantly. It was found that the yield strength of the SS-ECAP 1P sample was higher by ~42 % while the ultimate strength and the elongation were lower by ~5 % and ~34 %, respectively, by comparison with the as-received sample. The SS-ECAP 4P sample displayed a remarkably improved tensile strength where the yield and ultimate strengths were higher by ~67 % (~188 MPa) and ~4% (~16 MPa) than the as-received sample, respectively, while the elongation was lower by ~54 %.

After post-SS-ECAP aging, the ultimate strengths were reduced with similar ductility by comparison to that after SS-ECAP processing shown in Fig.1. This phenomenon is different from the

alloy in the T6 state before ECAP where a post-ECAP heat treatment increases the strength together with improving the ductility [18]. Additionally, the post-SS-ECAP aging has different effects on the yield strengths for the 1 pass and the 4 passes samples. The yield strength of the SS-ECAP 1P sample after post-ECAP aging increases slightly while it decreases to ~45 MPa in the SS-ECAP 4P sample after post-ECAP aging by comparison with the counterpart without post-ECAP aging.

3.2 Microstructure characterization after SS-ECAP processing

The microstructure of the as-received Al-Zn-Mg alloy was examined and characterized in an earlier report [19]. The average grain size of the as-received alloy was ~1.3 μm including heterogeneously distributed plate-like and near-spherical second phase particles, mainly of η' , with the presence of some limited η , T and E precipitates along the grain boundaries and within the grains. Detailed structure information of the different precipitates in the alloy were provided in the earlier report [19].

Typical micrographs of the SS-ECAP-processed Al-Zn-Mg alloy are shown in Fig. 2. Inspection of Fig. 2(a) shows that the microstructure after 1 pass of ECAP has a dislocation cell structure with dislocation tangles within the subgrains. The average equivalent grain size is ~800 nm for this condition. Numerous fine spherical precipitates that are well-distributed in the microstructure after 1 pass of ECAP are visible in Fig. 2 (b) in which indexing along $<114>_{\text{Al}}$ shows the precipitates are mainly G.P. zones along $1/3 \{220\}_{\text{Al}}$ and $1/2 \{113\}_{\text{Al}}$, η' along $\{123\}_{\text{Al}}$ and $\{135\}_{\text{Al}}$ with a very few η along $\{113\}_{\text{Al}}$. Spots of E along $\{440\}_{\text{Al}}$ and along $\{220\}_{\text{Al}}$ with the presence of T along $\{203\}_{\text{Al}}$ are also visible. The HRTEM and the selected area electron diffraction (SAED) pattern inserted in Fig. 2(b) reveals large numbers of fine spherical G.P. zones of ~3-5 nm in diameter and spherical and platelet η' precipitated through dynamic aging during the ECAP processing and homogeneously distributed within the Al matrix. The average size of these fine spherical precipitates is ~13 nm with a measured volume fraction of ~0.106. Figure 2(c) shows the presence of elongated fine grains with an average equivalent grain size

of ~300 nm after ECAP for 4 passes. The fine precipitates after 4 passes of ECAP shown in Fig. 2(d) are mainly of η' along $\{022\}_{\text{Al}}$ and $1/3\{022\}_{\text{Al}}$ with the presence of η along $\{111\}_{\text{Al}}$, E phase along $\{311\}_{\text{Al}}$, T phase along $\{203\}_{\text{Al}}$ and a weak spot of Al_3Zr along $1/2\{110\}_{\text{Al}}$. The size of the η' precipitates having a near-spherical morphology was slightly increased after 4 passes as depicted in the HRTEM inserted in Fig. 2(d) and the volume fraction of precipitates was slightly increased to ~0.112 having an average size of ~18 nm.

3.2 Microstructure characterization after post-SS-ECAP heat treatment

Figure 3 displays the microstructures of the post-SS-ECAP aged Al-Zn-Mg alloy (SS-ECAP-HT). Inspection of Fig. 3(a) shows the microstructure in the 1 pass sample consists mainly of elongated grains having average lengths of ~850 nm with the presence of dislocation tangles within some grains. Fine precipitates are homogeneously distributed in the Al matrix with the presence of overlapping coarse platelets as depicted in Fig. 3(b). The SAED pattern along $\langle 110 \rangle_{\text{Al}}$ shows the precipitates are mainly of η' with the presence of η , T and E phases with a volume fraction of ~0.11. The average size of the spherical precipitates is ~14 nm while the platelet precipitates have average lengths of ~120 nm. Aging of the 4 ECAP passes sample gives a slight increase in grain size with a mean size of ~360 nm and elongated grains that evolve partially into equiaxed grains as shown in Fig. 3(c) by comparison to the sample before aging as shown earlier in Fig. 2(c). A high density of dislocations and dislocation tangles are visible within the grains in Fig. 3(c) and the major precipitates are η' , η , T and E phases displayed along $\langle 013 \rangle_{\text{Al}}$ in Fig. 3(d) having a volume fraction of ~0.115. The average size of the precipitates has increased to ~20 nm for the near-spherical precipitates and ~110 nm in average length for the plate-like precipitate. It is apparent also that the plate-like precipitates are fewer in the SS-ECAP 4P-HT sample compared to the SS-ECAP 1P-HT sample as observed in Fig. 3. This is attributed to the larger numbers

of plate precipitates before aging in the SS-ECAP 1P sample compared to the SS-ECAP 4P sample which has more spherical particles as depicted in Fig. 2(b) and (d).

The dislocation densities were estimated by XRD and the values were $\sim 2.5 \times 10^{13}$, $\sim 2.8 \times 10^{14}$ and $\sim 2.9 \times 10^{14} \text{ m}^{-2}$ in the as-received and the SS-ECAP processed alloy after 1 and 4 passes, respectively. The dislocation density is slightly decreased after post-SS-ECAP aging with values of $\sim 2.6 \times 10^{14}$ and $\sim 2.7 \times 10^{14} \text{ m}^{-2}$ for the 1 pass and 4 passes samples, respectively. For convenience, the overall microstructural features of the as-received, the SS-ECAP processed and the SS-ECAP-HT processed Al alloy are summarized in Table 2.

An overlapping of precipitates was detected in the sample after post-SS-ECAP aging as observed in Fig. 3. In order to investigate the twining and coherency of these overlapped particles, several HRTEM observations were conducted on randomly selected particles. Two overlapping particles in the SS-ECAP 1P-HT sample are represented in Fig. 4 where Fig. 4 (a) shows the overlapped particles with several fine spherical particles close to the dislocation lines. Inspection of the corresponding FFT (Fast Fourier Transform) patterns in Fig. 4(b) shows that the oval-shaped particle has the orientation of the T phase along $(358)_{\text{Al}}$ while the plate-like particle is oriented along $(422)_{\text{Al}}$ with reflections of the E phase and with the presence of the η phase. Parallel spots were also observed in the FFT supporting the presence of twins within the particle as observed in Fig. 4(a).

To further examine the coherency of the interface, IFFT (Inverse Fast Fourier Transform) patterns in Fig. 4 (c) and (d) were obtained from the selected area presented in Fig. 4(a). It is readily apparent that the overlapping T and E phase are incoherent with the Al matrix as verified by the IFFT patterns. Further inspection of the two overlapping particles was performed by EDX as shown in Fig. 5. In Fig. 5(a) these precipitates contain a significant proportion of Al, Mg, Mn, Cr and a low percentage of Cu. It appears that the presence of these solutes within these overlapping phases has never been reported

previously in the 7xxx series alloys. In Fig. 5(b) the overlapping particles are shown after tilting along $<110>_{\text{Al}}$ and the corresponding EDX line scan is given in Fig. 5(c) which demonstrates that the overlapping phase is rich in Al, Mg, Cr and Mn with approximate ratios of 4:2:1:1 while the Mg-Zn-rich areas have Mg:Zn in the ratio of ~2:1 which supports the presence of η -type precipitates [24]. A similar phenomenon was found in the SS-ECAP 4P-HT sample as displayed in Fig. 6(a). In addition, fine particles are depicted as η precipitates in the coarse plate-like T phase detected by the FFT pattern in Fig. 6(b) and this demonstrates clearly that the interfaces between the Al matrix and the overlapping T phases are incoherent. The EDX mapping in Fig. 6(c) shows also the amounts of Al, Mg, Mn and Cr with a low percentage of Cu in the overlapped phases. It appears that the fine particles are probably of the η -type phase by inspection of the Mg:Zn ratio by EDX. The presence of different solutes and the nucleation of η within the overlapping particles is attributed to the occurrence of dislocation motion which acts to distribute the solute [25,26].

4. Discussion

4.1 Influence of post-SS-ECAP heat treatments on the tensile properties

A comparison of Figs 2 and 3 shows that after a post-SS-ECAP heat treatment there is a limited dislocation recovery with slight grain growth by comparison with the microstructure before the heat treatment. The delay in the recovery process is due to the high volume fraction of fine precipitates after ECAP processing which plays an effective role in pinning the dislocations and hindering grain boundary movement [27-29]. As a consequence, grain boundary and dislocation strengthening play only a limited role before and after the heat treatment. The differences in the strengths between the SS-ECAP samples and the SS-ECAP-HT sample are primarily due to the precipitate evolution during the post-SS-ECAP aging. The SS-ECAP 1P-HT sample shows a slight increase in the yield strength which is ascribed to the transformation of G.P. zones into η' and a volume fraction increase of the η' phase [30]. However, aging

of the SS-ECAP 4P sample causes a decrease in strength due to the slight increase in the size of the precipitates, the formation of larger plate-like precipitates with lengths of ~110 nm together with the transformation of η' to η during the post-ECAP heat treatment at 393 K for 20 h.

Figure 1 shows the SS-ECAP-HT samples have a lower ultimate strength by comparison with the SS-ECAP samples. The higher ultimate strength of the SS-ECAP 1P sample is due to the high work hardening rate. The true-stress-true strain curves show that all tested samples display high initial work hardening rates due to the large numbers of non-shearable T, E and η precipitates which trap dislocations and lead to dislocation pile-ups at the beginning of the tensile testing [31-32]. The initial work hardening rate is not sustainable at true strains over ~0.05 in the SS-ECAP 4P, SS-ECAP 1P-HT and SS-ECAP 4P HT samples owing to the high volume fractions of non-shearable precipitates. Therefore, with further straining the initial array of Orowan loops left by the dislocation movement will plastically relax under various mechanisms such as the nucleation and glide of prismatic dislocation loops around the particles [31]. In addition, overlapping of non-shearable precipitates along dislocations can assist in the recovery process of the SS-ECAP-HT samples by pinning and accumulation of dislocations followed by annihilation of opposite sign dislocation loops. The lower volume fraction of precipitates in the as-received and SS-ECAP-1P samples compared to the other tested samples and the additional presence of G.P. zones in these samples lead to a decrease in the volume fraction of the non-shearable precipitates in the microstructure. This gives a high work hardening rate which is attributed to the storage of additional geometrically-necessary dislocations and the storage of elastic energy [31].

4.2 Influence of pre-ECAP heat treatments on the tensile properties

The effect of ECAP processing and post-ECAP heat treatments at 393 K for 20 h on the tensile properties of the Al-Zn-Mg alloy with pre-ECAP in the T6 state were evaluated in an earlier report [18].

For convenience, the processing of the alloy by ECAP in the T6 state is designated as T6-ECAP and the processing of the alloy by ECAP and a post-ECAP heat treatment is designated as T6-ECAP-HT.

Table 3 displays tensile property data for the Al-Zn-Mg alloy under different processing conditions. It is apparent that for ECAP processing for 1 or 4 passes the T6-ECAP sample always has less strength and ductility than the SS-ECAP sample. By calculation, it was estimated that the yield strength, ultimate strength and ductility of the T6-ECAP 1P sample was lower by ~27 %, ~21 % and ~54 %, respectively, than for the SS-ECAP 1P sample and those of the T6-ECAP 4P sample were lower by ~36 %, ~29 % and ~8 % than the SS-ECAP 4P sample, respectively. The higher strengths and improved ductility of the SS-ECAP samples over the T6-ECAP samples is due to the higher volume fraction, smaller size and more homogeneously distributed precipitates in the SS-ECAP samples as shown in Fig.2.

The SS-ECAP samples were pre-ECAP heat treated at 743 K for 1 h and water cooled, so that precipitation by dynamic aging occurred during ECAP which resulted in a large number of nano-sized precipitates which were well-distributed in the Al matrix. However, as described previously [19,33], the fine precipitates after T6-ECAP processing came mainly from fragmented η' and a few T and E phases which existed in the matrix with sizes of ~120-180 nm before ECAP. This means that the homogeneity of the second phase distribution was much lower and the size was larger than after the SS-ECAP processing such that the average size of the precipitates was ~60 nm in the T6-ECAP 4P sample but only ~18 nm in the SS-ECAP 4P sample [18, 19].

Table 3 shows there is a slight increase in the yield strength of the SS-ECAP 1P-HT sample over the T6-ECAP 1P-HT sample. There are small differences in the grain sizes with precipitates mainly of η' , η , T and E in the two different processing conditions but nevertheless the increase can be attributed directly to the higher volume fraction of fine precipitates in the SS-ECAP 1P-HT samples over the T6-

ECAP 1P-HT samples [18, 19]. Thus, the strength of the SS-ECAP 4P-HT sample is higher than the T6-ECAP 4P-HT sample owing to the high volume fraction of fine η' , η , T and E precipitates in the SS-ECAP 4P-HT sample which are mainly of η with the presence of η' , T and E phases [18, 19]. The higher volume fraction of finer precipitates in the SS-ECAP-HT samples comes from the large number of fine precipitates formed by dynamic precipitation during plastic ECAP processing, where these precipitates coarsen slightly accompanied by the new nucleation of fine precipitates from the solutes remaining in the Al matrix during the post-SS-ECAP aging [34].

The SS-ECAP samples have improved ductilities over the T6-ECAP samples as shown in Table 3 and this is due to the higher volume fraction and finer precipitates in the SS-ECAP samples compared with the T6-ECAP samples. However, the SS-ECAP-HT samples have lower ductilities than the T6-ECAP-HT samples. The samples with pre-ECAP in the T6 state have T and E phases along the grain boundaries which stabilize the grain shape during ECAP processing and any post-ECAP heat treatment [35]. However, the SS-ECAP-HT has an elongated grain structure and this gives a low fracture resistance along the boundaries of the elongated grains and consequently a reduction in the overall ductility.

5. Summary and conclusions

1. ECAP processing enhances the yield strength of a supersaturated Al alloy and decreases the ductility. With an increase in the number of ECAP passes from 1 to 4, the yield strength further increases. A post-ECAP aging decreases the strength for the supersaturated alloy after 4 passes of ECAP but slightly increases the yield strength after 1 pass of ECAP.
2. For the supersaturated Al alloy, during ECAP processing for 1-4 passes the grains are refined, the dislocation density increases and there is dynamic aging precipitation. This dynamic aging forms large numbers of near-spherical precipitates which are well-distributed in the Al matrix with mean sizes

up to ~18 nm. During post-ECAP aging at 393 K for 20 h, there is a limited dislocation recovery with slight grain growth. The precipitate evolution leads to a slight increase in size and the formation of some larger plate-like precipitate with lengths of ~110-120 nm together with the transformation of G.P. zones into η' and η' to η . The overlapping of T and E precipitates after post-ECAP aging is incoherent with the matrix.

3. Due to the higher volume fraction, smaller size and more homogeneous distribution of precipitates in the alloy with pre-ECAP in the supersaturated state after ECAP processing compared with the alloy with pre-ECAP in the peak aging state, the strengths of the alloy with pre-ECAP in the supersaturated state are higher than with the pre-ECAP in the peak aging state both after ECAP processing and after the post-ECAP heat treatments.

Acknowledgements

This work was supported in part by the National Natural Science Foundation of China under Grant no. 51671030 and in part by the European Research Council under ERC Grant Agreement no. 267464-SPDMETALS.

References

- [1] H. Gleiter, Nanostructured materials: basic concepts and microstructure, *Acta Mater.* 48(2000) 1-29. doi:10.1016/S1359-6454(99)00285-2.
- [2] E.J. Lavernia, B.Q. Han, J.M. Schoenung, Cryomilled nanostructured materials: Processing and properties, *Mater. Sci. Eng. A.* 493 (2008) 207–214. doi:10.1016/j.msea.2007.06.099.
- [3] Y.T. Zhu, T.G. Langdon, The fundamentals of nanostructured materials processed by severe plastic deformation, *JOM* 56(10) (2004) 58–63. doi:10.1007/s11837-004-0294-0.
- [4] R.Z. Valiev, R.K. Islamgaliev, I. V. Alexandrov, Bulk nanostructured materials from severe plastic deformation, *Prog. Mater. Sci.* 45 (2000) 103-189. doi:10.1016/S0079-6425(99)00007-9.
- [5] R.Z. Valiev, T.G. Langdon, Principles of equal-channel angular pressing as a processing tool for grain refinement, *Prog. Mater. Sci.* 51 (2006) 881–981. doi:10.1016/j.pmatsci.2006.02.003.
- [6] A.P. Zhilyaev, T.G. Langdon, Using high-pressure torsion for metal processing: Fundamentals and applications, *Prog. Mater. Sci.* 53 (2008) 893–979. doi:10.1016/j.pmatsci.2008.03.002.
- [7] J. Gubicza, I. Schiller, N.Q. Chinh, J. Illy, Z. Horita, T.G. Langdon, The effect of severe plastic deformation on precipitation in supersaturated Al-Zn-Mg alloys, *Mater. Sci. Eng. A.* 460–461 (2007) 77–85. doi:10.1016/j.msea.2007.01.001.
- [8] K. Ma, H. Wen, T. Hu, T.D. Topping, D. Isheim, D.N. Seidman, E.J. Lavernia, J.M. Schoenung, Mechanical behavior and strengthening mechanisms in ultrafine grain precipitation-strengthened aluminum alloy, *Acta Mater.* 62 (2014) 141–155. doi:10.1016/j.actamat.2013.09.042.
- [9] L.J. Zheng, C.Q. Chen, T.T. Zhou, P.Y. Liu, M.G. Zeng, Structure and properties of ultrafine-grained Al-Zn-Mg-Cu and Al-Cu-Mg-Mn alloys fabricated by ECA pressing combined with thermal treatment, *Mater. Charact.* 49 (2002) 455–461. doi:10.1016/S1044-5803(03)00069-X.

- [10] L.J. Zheng, H.X. Li, M.F. Hashmi, C.Q. Chen, Y. Zhang, M.G. Zeng, Evolution of microstructure and strengthening of 7050 Al alloy by ECAP combined with heat-treatment, *J. Mater. Process. Technol.* 171 (2006) 100–107. doi:10.1016/j.jmatprotec.2005.06.049.
- [11] K.R. Cardoso, D.N. Travessa, W.J. Botta, A.M. Jorge, High strength AA7050 Al alloy processed by ECAP: Microstructure and mechanical properties, *Mater. Sci. Eng. A* 528 (2011) 5804–5811. doi:10.1016/j.msea.2011.04.007.
- [12] M.H. Shaeri, M.T. Salehi, S.H. Seyyedein, M.R. Abutalebi, J.K. Park, Microstructure and mechanical properties of Al-7075 alloy processed by equal channel angular pressing combined with aging treatment, *Mater. Des.* 57 (2014) 250–257. doi:10.1016/j.matdes.2014.01.008.
- [13] C.M. Cepeda-Jiménez, J.M. García-Infanta, E.F. Rauch, J.J. Blandin, O.A. Ruano, F. Carreño, Influence of processing severity during equal-channel angular pressing on the microstructure of an Al-Zn-Mg-Cu alloy, *Metall. Mater. Trans. A* 43A (2012) 4224–4236. doi:10.1007/s11661-012-1206-5.
- [14] Z.C. Duan, N.Q. Chinh, C. Xu, T.G. Langdon, Developing processing routes for the equal-channel angular pressing of age-hardenable aluminum alloys, *Metall. Mater. Trans. A* 41A (2010) 802–809. doi:10.1007/s11661-009-0020-1.
- [15] M.H. Shaeri, M. Shaeri, M. Ebrahimi, M.T. Salehi, S.H. Seyyedein, Effect of ECAP temperature on microstructure and mechanical properties of Al-Zn-Mg-Cu alloy, *Prog. Nat. Sci. Mater. Int.* 26 (2016) 182–191. doi:10.1016/j.pnsc.2016.03.003.
- [16] C.M. Cepeda-Jiménez, J.M. García-Infanta, O.A. Ruano, F. Carreño, Mechanical properties at room temperature of an Al-Zn-Mg-Cu alloy processed by equal channel angular pressing, *J. Alloys Compd.* 509 (2011) 8649–8656. doi:10.1016/j.jallcom.2011.06.070.

- [17] W.J. Kim, J.K. Kim, H.K. Kim, J.W. Park, Y.H. Jeong, Effect of post equal-channel-angular-pressing aging on the modified 7075 Al alloy containing Sc, *J. Alloys Compd.* 450 (2008) 222–228. doi:10.1016/j.jallcom.2006.10.151.
- [18] M.A. Afifi, Y.C. Wang, P.H.R. Pereira, Y. Huang, Y. Wang, X. Cheng, S. Li, T.G. Langdon, Effect of heat treatments on the microstructures and tensile properties of an ultrafine-grained Al-Zn-Mg alloy processed by ECAP, *J. Alloys Compd.* 749 (2018) 567–574. doi:10.1016/j.jallcom.2018.03.206.
- [19] M.A. Afifi, Y.C. Wang, P.H.R. Pereira, Y. Wang, S. Li, Y. Huang, T.G. Langdon, Characterization of precipitates in an Al-Zn-Mg alloy processed by ECAP and subsequent annealing, *Mater. Sci. Eng. A* 712 (2018) 146–156. doi:10.1016/j.msea.2017.11.091.
- [20] D.B. Williams, C.B. Carter, *Transmission electron microscopy: A textbook for materials science*, Springer, New York, 2009.
- [21] J. Gubicza, G. Ribárik, G.R. Goren-Muginstein, A.R. Rosen, T. Ungár, The density and the character of dislocations in cubic and hexagonal polycrystals determined by X-ray diffraction, *Mater. Sci. Eng. A* 309–310 (2001) 60–63. doi:10.1016/S0921-5093(00)01666-X
- [22] Y.H. Zhao, X.Z. Liao, Z. Jin, R.Z. Valiev, Y.T. Zhu, Microstructures and mechanical properties of ultrafine grained 7075 Al alloy processed by ECAP and their evolutions during annealing, *Acta Mater.* 52 (2004) 4589–4599. doi:10.1016/j.actamat.2004.06.017.
- [23] D.N. Seidman, E.A. Marquis, D.C. Dunand, Precipitation strengthening at ambient and elevated temperatures of heat-treatable Al(Sc) alloys, *Acta Mater.* 50 (2002) 4021–4035. doi:10.1016/S1359-6454(02)00201-X.
- [24] S.K. Maloney, K. Hono, I.J. Polmear, S.P. Ringer, The chemistry of precipitates in an aged Al-2.1Zn-1.7Mg at.% alloy, *Scr. Mater.* 41 (1999) 1031–1038. doi:10.1016/S1359-6462(99)00253-5.

- [25] R.M. Allen, J.B. Vander Sande, The oriented growth of precipitates on dislocations in Al-Zn-Mg - part I. Experimental observations, *Acta Metall.* 28 (1980) 1185–1195. doi:10.1016/0001-6160(80)90073-5.
- [26] R.K.W. Marceau, N. Tsafnat, D. Haley, S.P. Ringer, Solute diffusion characteristics of a rapid hardening Al-Cu-Mg alloy during the early stages of age hardening, *Metall. Mater. Trans. A* 41A (2010) 1887–1890. doi:10.1007/s11661-010-0252-0.
- [27] P.J. Apps, M. Berta, P.B. Prangnell, The effect of dispersoids on the grain refinement mechanisms during deformation of aluminium alloys to ultra-high strains, *Acta Mater.* 53 (2005) 499–511. doi:10.1016/j.actamat.2004.09.042.
- [28] O. Situdikov, T. Sakai, E. Avtokratova, R. Kaibyshev, Y. Kimura, K. Tsuzaki, Grain refinement in a commercial Al-Mg-Sc alloy under hot ECAP conditions, *Mater. Sci. Eng. A* 444 (2007) 18–30. doi:10.1016/j.msea.2006.06.081.
- [29] M. Gazizov, S. Malopheyev, R. Kaibyshev, The effect of second-phase particles on grain refinement during equal-channel angular pressing in an Al-Cu-Mg-Ag alloy, *J. Mater. Sci.* 50 (2015) 990–1005. doi:10.1007/s10853-014-8659-4.
- [30] S. Zhang, W. Hu, R. Berghammer, G. Gottstein, Microstructure evolution and deformation behavior of ultrafine-grained Al-Zn-Mg alloys with fine η' precipitates, *Acta Mater.* 58 (2010) 6695–6705. doi:10.1016/j.actamat.2010.08.034.
- [31] L.M. Cheng, W.J. Poole, J.D. Embury, D.J. Lloyd, The influence of precipitation on the work-hardening behavior of the aluminum alloys AA6111 and AA7030, *Metall. Mater. Trans. A* 34A (2003) 2473–2481. doi: 10.1007/s11661-003-0007-2.

- [32] W.J. Poole, X. Wang, D.J. Lloyd, J.D. Embury, The shearable-non-shearable transition in Al-Mg-Si-Cu precipitation hardening alloys: implications on the distribution of slip, work hardening and fracture, *Philos. Mag.* 85 (2005) 3113–3135. doi:10.1080/14786430500154935.
- [33] M.A. Afifi, P.H.R. Pereira, Y.C. Wang, Y. Wang, S. Li, T.G. Langdon, Effect of ECAP processing on microstructure evolution and dynamic compressive behavior at different temperatures in an Al-Zn-Mg alloy, *Mater. Sci. Eng. A.* 684 (2017) 617–625. doi:10.1016/j.msea.2016.12.099.
- [34] A. Deschamps, F. Bley , F. Livet , D. Fabregue, L. David, In-situ small-angle X-ray scattering study of dynamic precipitation in an Al-Zn-Mg-Cu alloy, *Philos. Mag.* 83 (2003) 677–692. doi:10.1080/0141861021000051091.
- [35] J.S. Vetrano, S.M. Bruemmer, L.M. Pawlowski, I.M. Robertson, Influence of the particle size on recrystallization and grain growth in Al-Mg-X alloys, *Mater. Sci. Eng. A.* 238 (1997) 101–107. doi:10.1016/S0921-5093(97)00445-0.

Figure captions

Fig. 1. True stress-true strain curves of the as-received, the ECAP processed and the post-ECAP heat treated Al-Zn-Mg alloy after solid solution treatment.

Fig. 2. TEM images of the supersaturated Al-Zn-Mg alloy processed by ECAP for (a) 1 pass, (b) 1 pass at higher magnification with corresponding SAED along $<114>_{\text{Al}}$, (c) 4 passes and (d) 4 passes at higher magnification with corresponding SAED along $<011>_{\text{Al}}$.

Fig. 3. TEM images of the supersaturated Al-Zn-Mg alloy processed by ECAP for different passes and post-ECAP aging at 393 K for 20 h: (a) ECAP for 1 pass, (b) ECAP for 1 pass at higher magnification with corresponding SAED along $<110>_{\text{Al}}$, (c) ECAP for 4 passes and (d) ECAP for 4 passes at higher magnification with corresponding SAED along $<013>_{\text{Al}}$.

Fig. 4. HRTEM images of the supersaturated Al-Zn-Mg alloy after ECAP processing for 1 pass and aging at 393 K for 20 h showing (a) fine spherical precipitate inside two overlapping particles, (b) the contact zone of the overlapping particles at higher magnifications with equivalent FFT patterns showing the types of these phases, (c) a selected IFFT pattern presenting dislocations in the Al matrix near the precipitate interface and (d) IFFT presenting the incoherency of the T with the Al matrix.

Fig. 5. (a) EDX map of the overlapping particles showing the presence of different solutes within these particles in the supersaturated Al-Zn-Mg alloy processed by ECAP for 1 pass and further aged at 393 K for 20 h (b) HAADF-STEM of the overlapping particles after tilting along $<110>$ and (c) the corresponding line EDX.

Fig. 6.(a) TEM images of the supersaturated Al-Zn-Mg alloy processed by ECAP for 4 passes and further aged at 393 K for 20 h with overlapping particles along array of dislocations, (b) selected area in (a) presence of fine particles marked by arrows and (c) EDX maps of the overlapping particles.

Table captions

Table.1. Sample designation of the Al-Zn-Mg alloy and corresponding processing parameters.

Table.2 Summary of microstructural features tested in the as-received, SS-ECAP processed and SS-ECAP-HT processed Al-Zn-Mg alloy.

Table.3. Tensile properties data of the Al-Zn-Mg alloy at different processing conditions.

Table.1. Sample designation of the Al-Zn-Mg alloy and corresponding processing parameters.

Sample	Processing condition
As-received	Solid solution treatment at 743 K for 1 h and then aging at 393 K for 24 h
SS-ECAP 1P	Solid solution treatment at 743 K for 1 h + ECAP processing for 1 pass
SS-ECAP 4P	Solid solution treatment at 743 K for 1 h + ECAP processing for 4 passes
SS-ECAP 1P-HT	Solid solution treatment at 743 K for 1 h + ECAP processing for 1 pass + aging at 393 K for 20 h
SS-ECAP 4P-HT	Solid solution treatment at 743 K for 1 h + ECAP processing for 4 passes + aging at 393 K for 20 h

Table.2 Summary of microstructural features tested in the as-received, SS-ECAP processed and SS-ECAP-HT processed Al-Zn-Mg alloy.

		As-received	SS-ECAP1P	SS-ECAP4P	SS-ECAP1P-HT	SS-ECAP4P-HT
Grain size		1.3 μm	800 nm	300 nm	L \approx 850 nm	360 nm
Precipitates	Type	G.P., η' , η , T & E	G.P., η' , η , T & E	η' , η , T & E	η' , η , T & E	η' , η , T & E
	Size (nm)	G.P. \sim 5, η' \sim 120, T&E \sim 180	D \sim 13	D \sim 18	D \sim 14 L \sim 120	D \sim 20 L \sim 110
	Morphology	Spherical/ Platelet	Spherical/ few Platelet	Spherical	Spherical/ Platelet	Spherical/ Platelet
	Volume fraction %	3.1	10.6	11.2	11	11.5
Dislocation density (m^{-2})		2.5×10^{13}	2.8×10^{14}	2.9×10^{14}	2.6×10^{14}	2.7×10^{14}

Table.3. Tensile properties data of the Al-Zn-Mg alloy at different processing conditions.

Sample	0.2% Yield strength (MPa)	Ultimate tensile strength (MPa)	Elongation (%)
As-received (T6)	281	485	20
T6-ECAP 1P	314	385	7[18]
SS-ECAP 1P	398	465	15
T6-ECAP 4P	347	390	12[18]
SS-ECAP 4P	469	501	13
T6-ECAP 1P-HT	376	440	17[18]
SS-ECAP 1P-HT	407	429	12.5
T6-ECAP4P-HT	362	414	17 [18]
SS-ECAP4P-HT	424	469	13

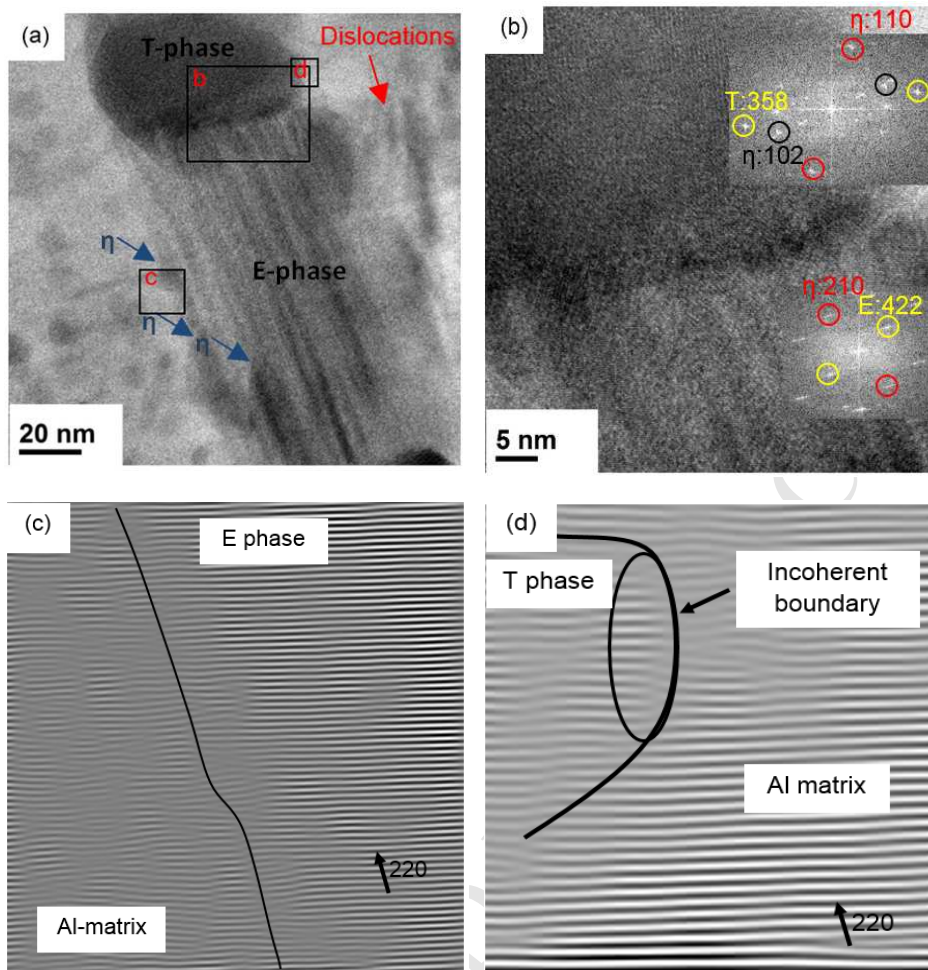


Fig. 4. HRTEM images of the supersaturated Al-Zn-Mg alloy after ECAP processing for 1 pass and aging at 393 K for 20 h showing (a) fine spherical precipitate inside two overlapping particles, (b) the contact zone of the overlapping particles at higher magnifications with equivalent FFT patterns showing the types of these phases, (c) a selected IFFT pattern presenting dislocations in the Al matrix near the precipitate interface and (d) IFFT presenting the incoherency of the T with the Al matrix.

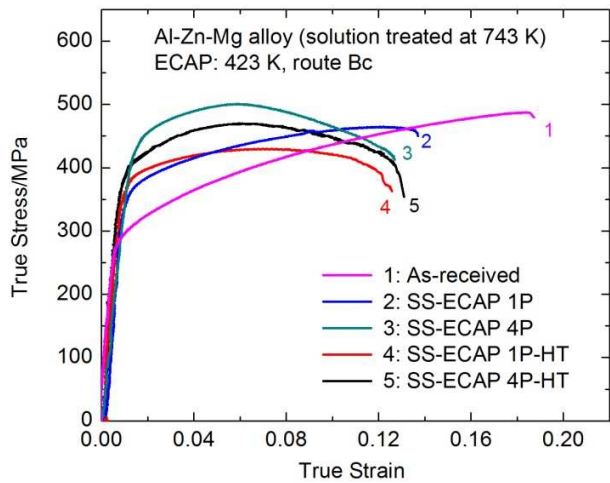


Fig. 1. True stress-true strain curves of the as-received, the ECAP processed and the post-ECAP heat treated Al-Zn-Mg alloy after solid solution treatment

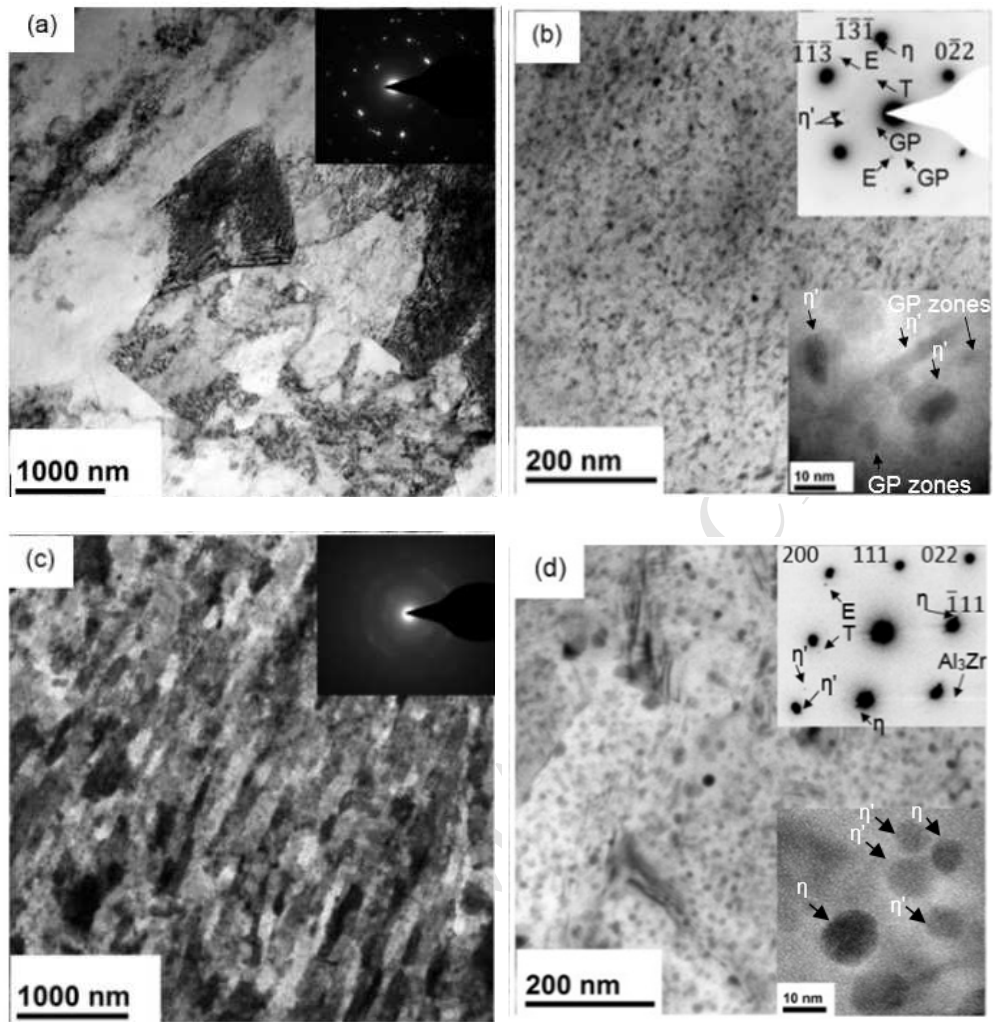


Fig. 2. TEM images of the supersaturated Al-Zn-Mg alloy processed by ECAP for (a) 1 pass, (b) 1 pass at higher magnification with corresponding SAED along $<114>_{\text{Al}}$, (c) 4 passes and (d) 4 passes at higher magnification with corresponding SAED along $<011>_{\text{Al}}$.

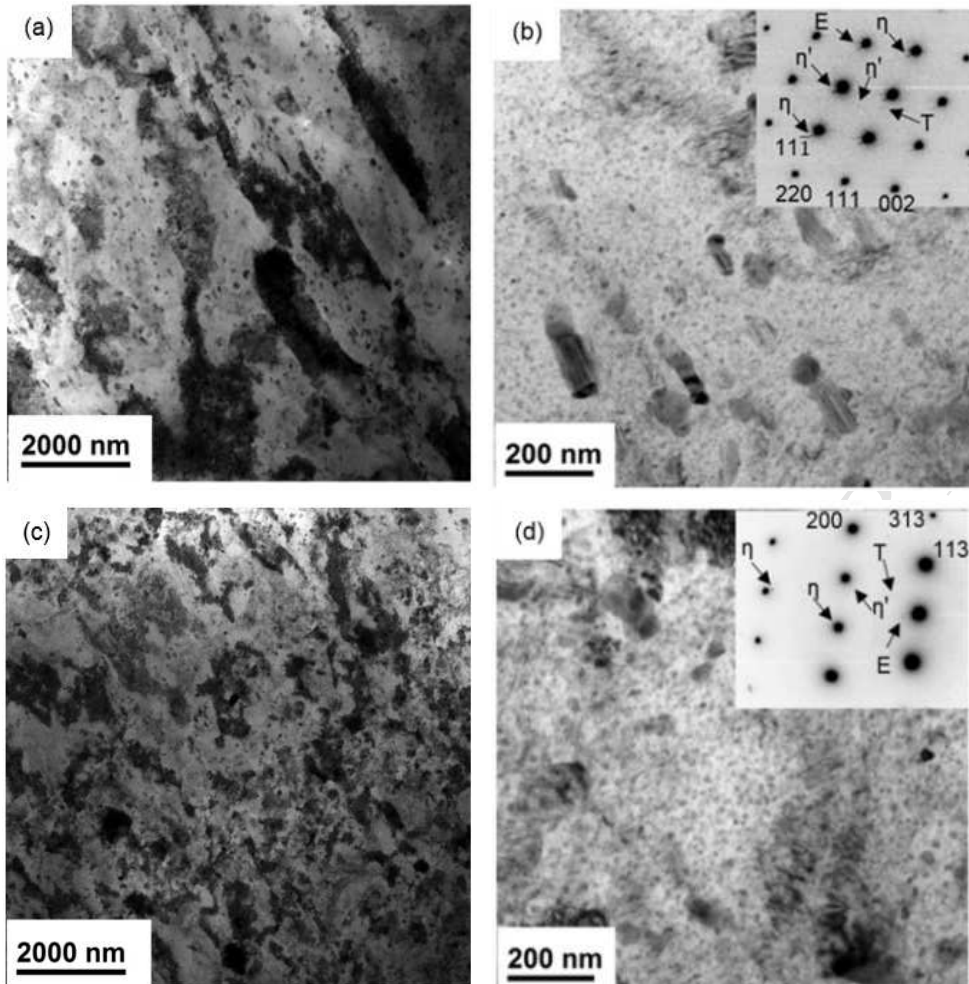


Fig. 3. TEM images of the supersaturated Al-Zn-Mg alloy processed by ECAP for different passes and post-ECAP aging at 393 K for 20 h: (a) ECAP for 1 pass, (b) ECAP for 1 pass at higher magnification with corresponding SAED along $<110>_{\text{Al}}$, (c) ECAP for 4 passes and (d) ECAP for 4 passes at higher magnification with corresponding SAED along $<013>_{\text{Al}}$.

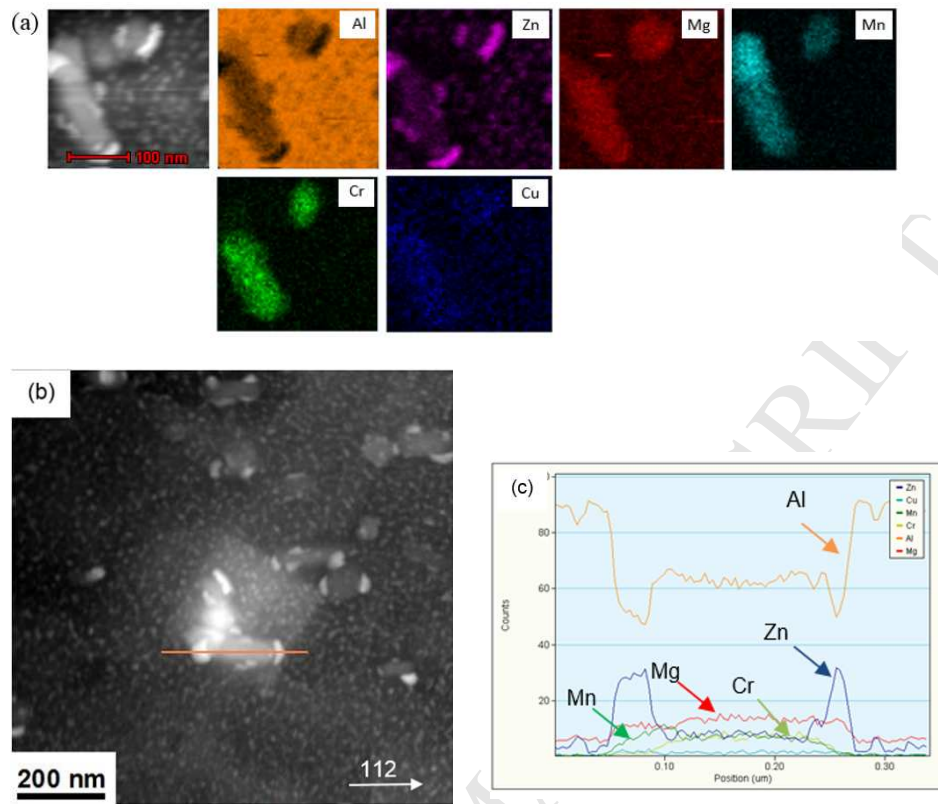


Fig.5. (a) EDX map of the overlapping particles showing the presence of different solutes within these particles in the supersaturated Al-Zn-Mg alloy processed by ECAP for 1 pass and further aged at 393 K for 20 h (b) HAADF-STEM of the overlapping particle after titling along <110> and (c) the corresponding line EDX.

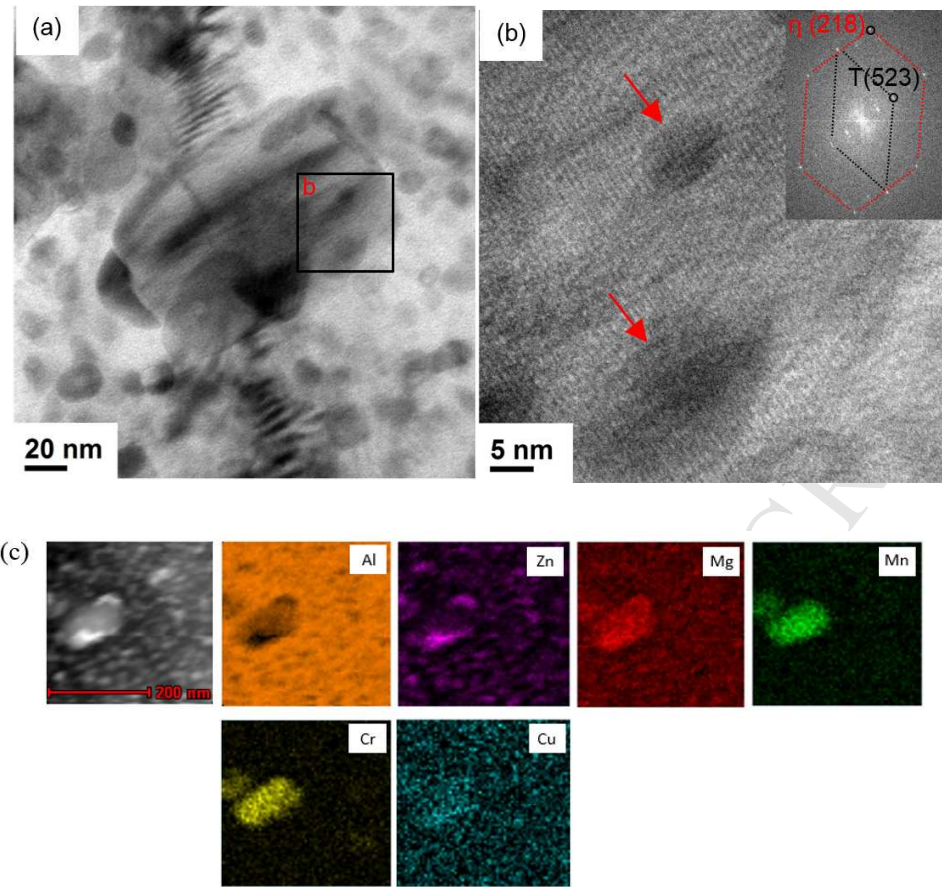


Fig. 6. (a) TEM images of the supersaturated Al-Zn-Mg alloy processed by ECAP for 4 passes and further aged at 393 K for 20 h with overlapping particles along array of dislocations, (b) selected area in (a) presence of fine particles marked by arrows and (c) EDX maps of the overlapping particles.

Highlights

- ECAP processing enhances yield strength of supersaturated Al-Zn-Mg.
- Post-ECAP aging decreases strength for the supersaturated alloy after 4 passes.
- During ECAP processing dynamic aging precipitation occurs
- Pre-ECAP heat treatments affect the strength of the alloy after ECAP processing
- Pre-ECAP heat treatments also affect the strength after post-ECAP heat treatments